

Reservoir And Elastic Property Prediction Away From Well Control

Kyle T. Spikes and Jack P. Dvorkin; Stanford Rock Physics Laboratory

Abstract

The ultimate goal of this effort is to quantify lithology, fluid, and porosity from seismic data. We approach this goal by generating synthetic seismograms and comparing them to real seismograms, with the expectation that a similarity in the seismic response indicates a similarity in the underlying rock properties, specifically, lithology, fluid, and porosity (LFP). The synthetic seismic approach also can be used to understand the sensitivity of real data to LFP. The starting point for synthetic seismic generation is rock physics analysis and geologic interpretation of well data. Then a geological model of the subsurface with geobodies and expected depositional and diagenetic patterns outlined. Next, geobodies are populated with clay content and the corresponding porosity and hydrocarbon saturation at the well log scale. These rock properties are translated into the P- and S-wave velocity and bulk density by using a rock physics model. Then synthetic seismograms are produced from the elastic properties. We illustrate this methodology using well data from a fluvial environment in which the clay content is related directly to the total porosity by the dispersed clay model and to oil content via irreducible water saturation. These properties are related to the velocity and density by the Raymer-Greenberg-Castagna model, which is appropriate for mature sand/shale sequences. We use standard schemes of depositional models to construct a vertical geological section of grain size distributions, with a fluvial channel that includes the well. We examine two – the massive and gradational – depositional sequences within the channel. In the case under examination, synthetic seismic appears to be sensitive to lithology, fluid, and porosity. This result indicates that LFP information can be extracted from real seismic.

Introduction

The depositional environment, diagenesis, burial, and compaction can vary substantially within the same basin or within the same stratigraphic facies. These factors may directly affect lithology, fluid, and porosity (LFP). LFP, in turn, affects the elastic properties of the rock and, subsequently, the seismic response. The main question of exploration is how to translate seismic data into LFP.

Our approach to this problem is synthetic seismogram generation and comparison thereof to real seismic data. If the real and synthetic data are similar, we assume a similarity in the underlying LFP. Of course, this approach carries non-uniqueness because multiple combinations of reservoir properties and geometries can produce the same seismic signature. However, the power of the synthetic seismic approach is that responses can be generated easily, rapidly, and massively for various scenarios of lithology, porosity, and fluid distributions in the subsurface. By so doing, the geophysicist can create a site-specific catalogue of seismic signatures to assess various possibilities and probabilities contained in the field data. Also, synthetic seismic data helps to understand the sensitivity of real data to LFP.

Well data represent the rock properties along a one-dimensional spatial trajectory. Therefore, information contained in the well data lacks lateral continuity and cannot be used alone for reliable predictions of rock properties where

lateral geologic variation is significant.

Seismic amplitude data augments well data by providing information about the subsurface away from the well but at a much larger scale than well data. One powerful approach to mapping seismic-scale lithofacies away from well control is statistical rock physics^{1,2}. In this approach lithofacies are identified at a well, their seismic signatures, such as AVO are modeled, and synthetic seismic attributes, such as the intercept and gradient, are created and mapped into the seismic attribute space. A rock physics model then transforms the seismic amplitude or impedance into rock properties based on the seismic facies. In another current example³ neural networks are used to calibrate the elastic to reservoir properties at a well and then apply these statistically derived transforms to seismic inversion volumes.

We build upon this approach by deterministically generating pseudo-wells and the corresponding synthetic seismic data for site-specific geological scenarios, not necessarily reflected in available well data. The first step is to establish a rock physics model at the calibration well that quantitatively explains the data. The second step involves building a geological model of the subsurface. This model can be based on a geological interpretation of the seismic amplitude volume or simply on the knowledge of the depositional environment around a well and assumptions about the shape and interval architecture. Once the expected depositional and diagenetic trends are identified, the geobodies are populated with clay content at the well-log scale according to standard and predictable depositional patterns⁴. In this particular case, clay content is equated to shale content (or grain-size distribution). In general, shale content does not equal clay content. However, in this study we equate the two, which is justified by rock physics relations present in the log data.

After the geobodies are populated with clay content, total porosity and hydrocarbon saturation values are assigned. In this example, both the total porosity and the hydrocarbon saturation are related directly to the clay content via the dispersed clay model and capillary pressure, respectively. Next, the rock physics model established at the well is used to obtain the P- and S-wave velocity and density from porosity, fluid, and mineralogy. Lastly, synthetic seismograms are generated to assess the effects of LFP, reservoir geometry, and lateral position on seismic signatures.

This methodology automatically generates pseudo-wells with an accompanying suite of log curves at any spatial trajectory within the geologic section from clay content only. Using clay content only for rock property and seismic velocity prediction is not a new approach⁵. Furthermore, the concept of pseudo-wells is not new. For example, Monte Carlo simulation is used to generate well data that account for the possible stratigraphic and physical property variability of a target interval⁶. Rock physics relations are used to construct pseudo-log data where the original data were missing due to borehole conditions⁷. We make a next step and combine rock physics with site-specific principles of deposition. We expect this approach to reduce uncertainty further in seismic interpreta-

tion.

Methodology

The methodology consists of five main steps. The first step is rock physics diagnostics of the well data to establish relations between LFP and the elastic properties of the rock. Secondly, we construct a synthetic geologic model based on a calibration well and standard depositional schemes. Thirdly, the geobodies are populated with clay content, porosity, and hydrocarbon saturation values. The fourth step is to apply a rock physics model established at the well to translate LFP into the density and elastic properties. Finally, synthetic seismograms and attributes are generated from the elastic properties.

Rock Physics Diagnostics. The rock physics diagnostics is performed to determine a model that quantitatively explains the well data shown in Figure 1. First, we apply Gassmann⁸ fluid substitution, or P-wave only substitution⁹ if S-wave data are unavailable or of questionable quality, to bring all data to 100% brine saturation. Then the impedance (I_p) and Poisson's ratio (ν) are plotted versus the total porosity (ϕ) and color-coded by gamma ray (GR) to highlight the lithology (Figure 2). Superimposed on the data are curves (blue) corresponding to clay content values of 0% to 100% in increments of 20% from the Raymer et al.¹⁰ model, $V_p = V_m(1-\phi)^2 + V_f\phi$, where V_m is the velocity in the mineral phase and V_f is the velocity in the pore fluid. The S-wave velocity is calculated from the Raymer et al.¹⁰ P-wave velocity by the Greenberg-Castagna¹¹ transform, which, in water-saturated, clastics is close to the mudrock equation $V_s = 0.862V_p - 1.172$ ¹². The bulk density (ρ_b) is $\rho_b = \rho_m(1-\phi) + \rho_f\phi$, where ρ_m is the density of the mineral phase, and ρ_f is the density of the pore fluid.

The Raymer-Greenberg-Castagna model suitably describes this data and, therefore, is appropriate for the rock under examination. The Raymer et al.¹⁰ model was derived for consolidated sediments. The fact that it matches the data means implicitly that we are dealing with a mature and consolidated sand/shale sequence.

For comparison, a line for 0% clay from the soft sand/shale model¹³ is plotted (gray). This model significantly underestimates I_p and overestimates ν . These inaccurate estimates confirm further that the sequence is mature and consolidated.

The $I_p - \phi$ cross-plot in Figure 2 is our guide to estimate the clay-content (C) from GR . We observe that the sand data with the smallest GR is matched by the $C=0.07$ Raymer et al.¹⁰ curve, whereas the shale data with the largest GR is matched by the $C=0.93$ curve. We use these bounds to scale the GR curve linearly to calculate C (Figure 1).

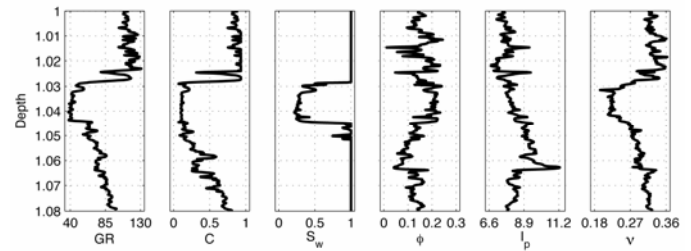


Figure 1. Calibration well log data from a fluvial dominated beach environment. The combined Raymer-Greenberg-Castagna rock physics model quantitatively explains this data.

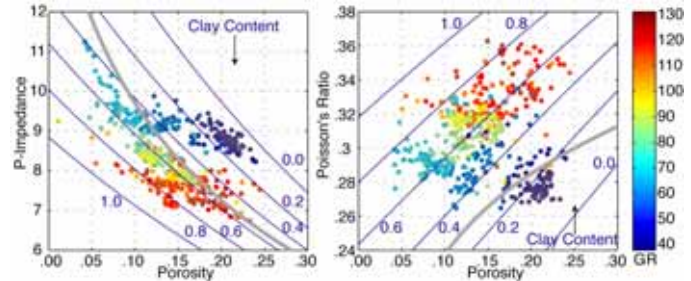


Figure 2. The P-wave impedance (left) and Poisson's ratio (right) versus the total porosity. The elastic properties are calculated for 100% water saturation. The data are color-coded by the gamma ray. The blue curves are from the combined Raymer-Greenberg-Castagna model, each drawn for a fixed clay content starting at 0.0 and ending at 1.0 with 0.2 step (clay content is shown on the curves). The bold gray curves are from the uncemented sand/shale model drawn for zero clay content. Notice that Poisson's ratio in the clean sand, as displayed here, is larger than the measured Poisson's ratio as displayed in Figure 1. This is because the Poisson's ratio here is calculated for 100% water saturated sand.

Geologic Model. The geologic interpretation of the well data in Figure 1 is that of a fluvial-dominated beach environment (similar to¹⁴). This interpretation is based on the clay content curve derived from the gamma ray curve. Seismic amplitude or impedance data can be used in addition to the calibration well data to determine the depositional environment and outline the geometry for the geobodies (e.g.,¹⁵). However, in this demonstration, we use well data exclusively.

After determining the depositional environment, the next step is to construct a vertical geological section. Six different facies are selected in the well based on clay content, and each corresponds to a different petrophysical facies¹⁶. Those facies (Figure 3, left) and their depositional settings include (I) a deep-water shale from 1 to ~1.027 depth; (II) a fluvial channel arenite between depths ~1.027 and ~1.045; (IIIA) a down-fining sequence between ~1.045 and ~1.058 depth grading vertically from a wacke to a shale; (IIIC) a second more clay-rich down-fining wacke to shale, from ~1.064 to ~1.08 depth; (IVA) a thin wacke lens at depth ~1.025; and (IVB) a wacke from an intermediate depth stationary stand between depths ~1.058 and ~1.064. Each of the down-fining sequences corresponds to relative changes in water level from deepest at the base of each sequence and shallowest at the top.

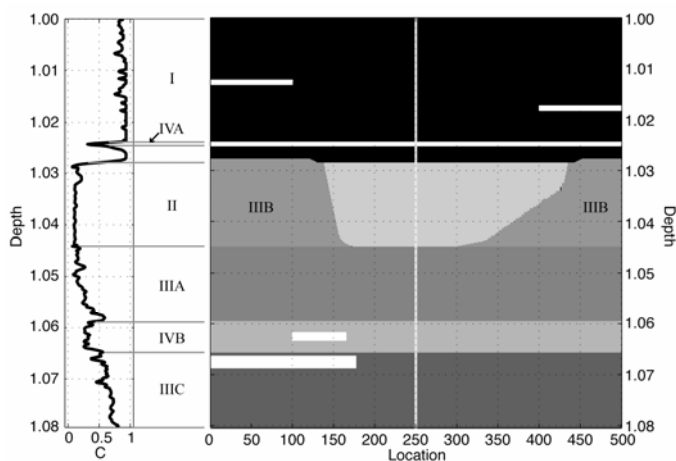


Figure 3. Facies model constrained by the calibration clay content log (left) whose location is indicated by the vertical line in the center of the model. Each of the facies corresponds to a different petrophysical facies¹⁶: (I) Shale; (II) arenite; (IIIA), (IIIB), and (IIIC) wacke grading downward to shale; (IVA) and (IVB) wacke.

Next, schematic geologic models^{17,18} associated with the depositional environment are combined with the selected facies to produce a synthetic vertical geological section of the facies (Figure 3, right). The overall vertical thickness of the model equals the vertical extent of the well data, and the horizontal extent is approximately the same as the vertical extent. The calibration well data are placed in the center of the model to control the thicknesses of the facies in the center of the model.

Each facies, except the arenite, is extended laterally to the edges of the model. The placement, geometry, and width of the channel is subject to stratigraphic interpretation of seismic data. In this specific case, we assume that the calibration well is located in the thickest part of the channel, and that the width is of the same order of magnitude as the thickness. To fill the model on the lateral sides of the channel, an additional down-fining wacke (Facies IIIB) is added to the model even though this facies is not present in the calibration well. The upper boundary of this facies extends above the top of the channel on both sides. Geologically, it is unlikely, that the bottom of this facies coincides with the bottom of the channel, but the placement of the lower boundary is not critical for this demonstration. Lastly, additional sand lenses are placed randomly in the model to simulate natural geological variability. At all locations, except the center of the model, the thickness, lateral extent, and lithology of each facies is based on subjective geologic interpretation. However, the geometries defined for the model are all geologically plausible.

Lithology, Fluid, and Porosity. The next step is to populate the geologic model with clay content, total porosity, and hydrocarbon saturation. For each of the facies, the clay content mean and standard deviation are determined from the calibration well (the clay content frame, Figure 1), and a normal distribution of clay content is assumed within each facies. It is then assumed that those statistical values are representative of the entire facies. For the down-fining sequences, the normal distribution of clay content is superimposed upon a uniform down-fining trend.

Based on schematic geologic models,^{17,18} two plausible depositional sequences are possible within the channel (Figure 4). In each case, clay content at the well location is preserved. The first scenario is a massive arenite that fines upward slightly. The second is, from left to right, a gradational arenite to wacke to shale sequence. For the second scenario, the clay content increases in the thinning part of the channel beyond the statistical range in the well.

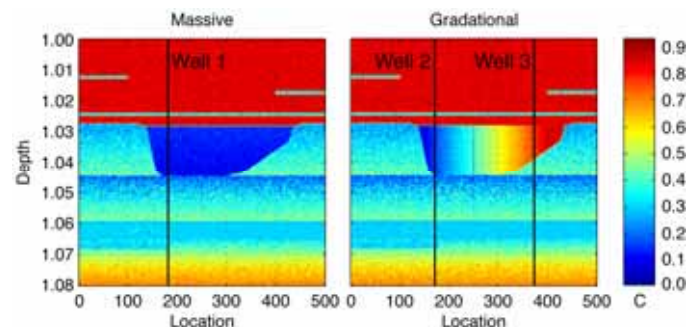


Figure 4. Clay content models derived from the data statistics in the calibration well and the geometry defined by the facies model in Figure 3. Clay content in each of the facies is shown by the color bar. The black lines are the pseudo-well locations selected for the sensitivity analysis.

The V-shaped pattern observed in the porosity-clay content cross-plots (Figure 5) indicates that these two properties are related to each other by the dispersed clay model, in which the small clay grains and the large sand grains are mixed at the pore scale^{19,20}. The total porosity of the two end-members (the sand and clay) are almost the same. However, the placement of the small grains into the pore space between the large grains results in smaller porosity at intermediate clay contents.

Dvorkin and Gutierrez²¹ and Spikes and Dvorkin²² propose a linear clay-content porosity trend for each of the two branches of the V to predict porosity from clay content. We take a similar approach here. For facies I, II, IIIA, and IIIC, best-fit linear trends between clay content and porosity are identified (Figure 5) and then used in the geological model to calculate the total porosity from clay content. Because the number of data points in Facies IVA and IVB is insufficient to draw any statistical relation, we use the IIIA trend for IVB, and the IIIC trend for IVA.

The validity of such linear C to ϕ transforms is not universal due to several factors. First, the assumption that GR can be linearly transformed into C is not always valid. GR is a measure of the natural radioactivity, not of particle size. For example, Potassium feldspar particles can increase the GR count in sands to the levels expected for pure shale or clay. This will act to underestimate the total porosity using this method. Conversely, small clay-size particles that are not clay, such as organics, will not contribute to the GR count. Then the total porosity will be overestimated.

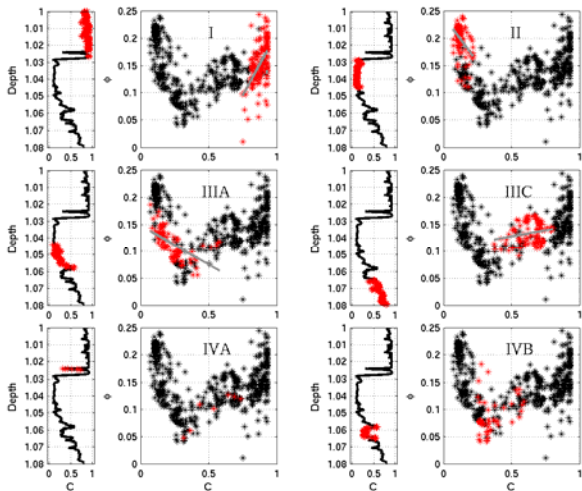


Figure 5. Lithologic facies interpreted from the clay content log are displayed versus depth and also in the porosity-clay content domain. Best-linear-fit lines are drawn for Facies I, II, IIIA, and IIIC.

The last part of generating LFP profiles is the calculation of water saturation (S_w) as a function of clay content. In many sediments, S_w is a function of grain size simply because smaller grains in water-wet rock cause larger capillary forces and thus prevent the displacement of water by hydrocarbons. This fact is implicitly contained in the commonly used permeability equations. The Kozeny-Carman²³ class of equations relates the absolute permeability to the grain size squared. The Tixier²⁴, Wyllie and Rose²⁵, and Timur²⁶ class of equations relates permeability to the irreducible water saturation. Therefore, S_w is related to the grain size and, in our case, to C .

We find an appropriate $S_w - C$ relation in the calibration data. In Figure 1, the S_w , as derived from the resistivity log, varies between 0.2 and 0.3 in arenite channel and is 1 elsewhere. A cross plot of S_w versus C in Figure 6 shows two relatively separate domains. For clay content larger than approximately 0.2, most of the S_w values are 1. We use the best linear fit for the points where $C \leq 0.2$ and $S_w \leq 0.5$, and fix $S_w = 1$ for $C > 0.2$ (Figure 6). This transform is used throughout the geologic cross-sections shown in Figure 4.

This treatment of S_w accounts for the immobile water in rock. In terms of predicting S_w from the clay content geologic cross-section, the above cutoff criterion serves to discriminate the arenite channel, where S_w is a linear function of C , from wackes and shales in which $S_w = 1$.

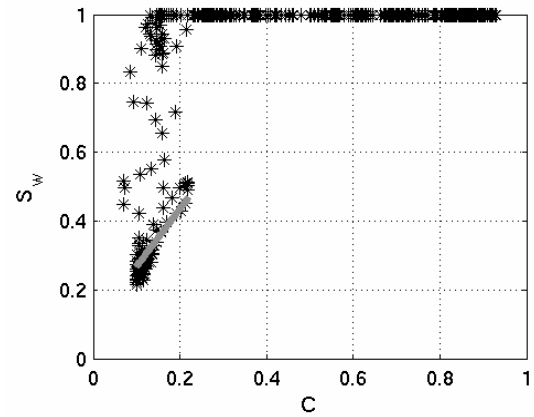


Figure 6. Water saturation versus clay content from the calibration well data. The linear trend (gray) was used to calculate water saturation as a function of clay content in the geologic cross-section.

Elastic Property Calculation. The fourth step is to calculate the density and P- and S-wave velocity from LFP. Rock physics diagnostics indicates that the Raymer-Greenberg-Castagna model quantitatively explains the calibration well data. Therefore, this model is used to calculate the elastic properties from the lithology, fluid, and porosity at any location in the geologic model.

Synthetic Seismogram and Seismic Attribute Calculation.

The fifth and final step is to use the elastic properties to generate synthetic seismograms. Reflectivity coefficients at incidence angles from 0 to 40 degrees are calculated using the Hilterman²⁷ approximation to the Zoeppritz²⁸ equations. Then a 40-Hz Ricker wavelet is convolved with the reflectivity series at all angles to produce a full AVO gather.

One reason for simulating a full gather is that the log curves in Figure 1 indicate a small contrast in the impedance but a strong Poisson's ratio contrast between the arenite and shale. We expect that this will be reflected in the far-offset traces.

Various seismic attributes, such as the intercept and gradient, can be calculated from synthetic seismograms. In this case we use only two attributes for illustration purposes: a pseudo-impedance and pseudo-Poisson's ratio. The first is calculated versus the two-way travel time (TWT) as the integral of the zero-offset trace. The second is extracted from a far-offset trace by resolving the Hilterman²⁷ approximation $R_{pp}(\theta) = R_{pp}(0)\cos^2\theta + 2.25\Delta v\sin^2\theta$ for Δv , where θ is the angle of incidence and R_{pp} is the P-to-P reflectivity.

In summary, we find that V_p , V_s , and ρ_b can be calculated directly from the clay content, total porosity, and pore fluid. We also find that clay content is directly responsible for porosity and pore fluid. Because of these relationships and because clay content is the main manifestation of the depositional regime, we find it essential to start with populating the model with clay content in order to produce geologically driven synthetic seismograms.

Pseudo-Wells and Synthetic Seismic Traces

We illustrate our methodology on the geologic models shown in Figure 4. First, we explore the effect of the pore fluid on the seismic response in a pseudo-well in the massive channel as shown in Figure 4, left (marked as Well 1). In the first scenario, the channel is saturated with oil, whereas in the alternative scenario, it is saturated with brine. The only difference between the two pseudo-wells is in water saturation; C and ϕ are the same.

The pseudo-log data and corresponding synthetic seismic traces for this well with oil and brine are shown in Figure 7, top and bottom, respectively. In both the oil- and brine-saturated cases, I_p and ν are calculated according to the Raymer-Greenberg-Castagna model. The results are essentially the same as those due to Gassmann⁸ or Mavko et al.⁹ fluid substitution of oil to brine.

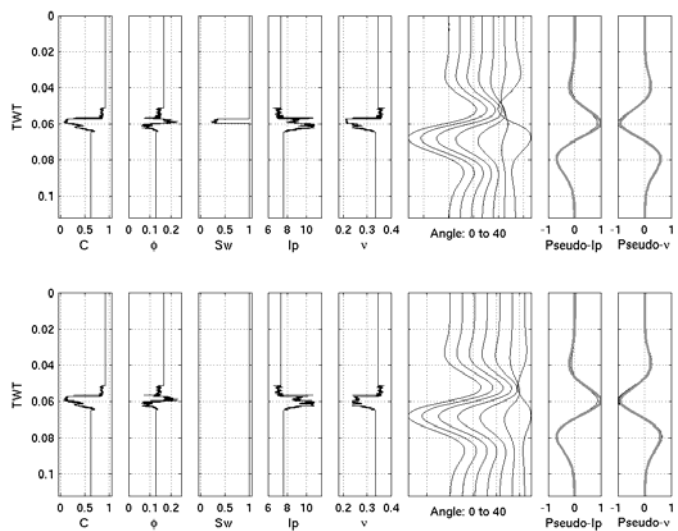


Figure 7. Synthetic log, seismic, and attribute data for pseudo-well 1 shown in Figure 4, left. The fluid was changed from oil (top row) to brine (bottom row) in the channel, as reflected in the water-saturation curves. The change of fluid subtly affects the far-offset traces. The seismic attributes change only slightly from the oil-saturated (black) to brine-saturated (gray) case. The two upper right and two lower right frames are identical.

Replacing hydrocarbon for brine results in only a slight change in I_p , but a larger, but still small, change in ν . As a result, the far-offset traces (incidence angles greater than 30 degrees) show a subtle change between the hydrocarbon and brine cases. The seismic attributes are displayed in Figure 7, right. The black lines correspond to the hydrocarbon-saturated case, and the gray lines are from the brine-saturated case. For display and comparison, the two pseudo- I_p traces are normalized by the global maximum of both pseudo- I_p traces. Similarly, each pseudo- ν trace is normalized by the global maximum of both pseudo- ν traces. As is evident in the attribute plots, very little difference exists between the attributes in the hydrocarbon- and brine-saturated cases. This is because the sand is consolidated, and thus its elastic properties are only weakly dependent on the compressibility and density differ-

ence between oil and brine.

The effect of the reservoir thickness on the seismic response is explored by doubling the thickness of the geologic model at the same pseudo-well location. Figure 8 displays the pseudo-log data, synthetic seismograms and attributes for the hydrocarbon- and brine-saturated cases. The exposition is the same as in Figure 7. In this case, the channel appears to be better resolved by pseudo- I_p and pseudo- ν . Still, only subtle differences exist between the oil and brine cases.

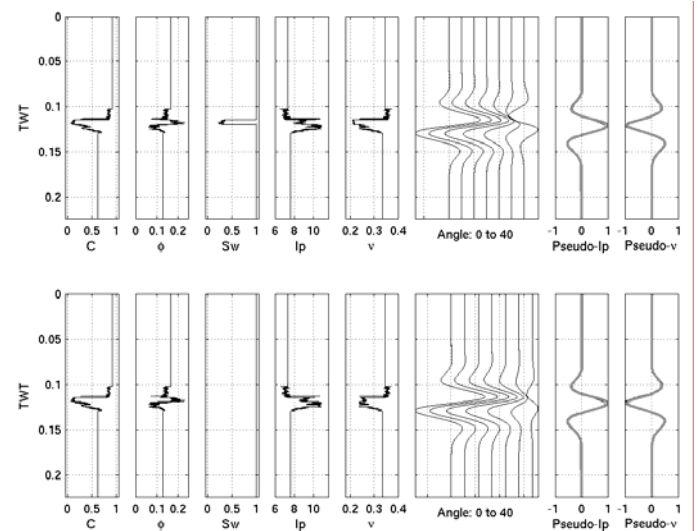


Figure 8. Same as Figure 7, except the thickness of the model is doubled.

The next stage is to demonstrate the combined effect of LFP on seismic response. Two pseudo-well locations are selected in the gradational clay model (Figure 4, right). Well 2 passes through a hydrocarbon-saturated arenite part of the channel, and Well 3 extends through a brine-saturated shale section of the channel. The pseudo-log data and seismograms corresponding to Well 2 are displayed in the top row of Figure 9, and the data from Well 3 are shown in the bottom row. Clay content in the channel increases from 5–15% to 80–90% from Well 2 to Well 3; the resulting ϕ decreases according to the linear trend for Facies I; and s_w becomes 1 in Well 3. These changes in C , ϕ , and s_w between the two pseudo-wells result in significantly different I_p and ν .

The resulting synthetic seismic traces from the two wells are noticeably different at the largest angles of incidence. The seismic attributes from the two well data show differences as well. As expected, each of the pseudo- I_p attribute traces mimics its corresponding I_p log, and the pseudo- ν attribute traces follow the general trends of the respective ν logs.

The observed difference in the seismic response illustrates our finding that the lithology, porosity, and water saturation may change together – an increase in C triggers a decrease in ϕ and increase in s_w (Figures 5 and 6). Such relations, if proven valid in a prospect area, may help constrain seismic interpretation.

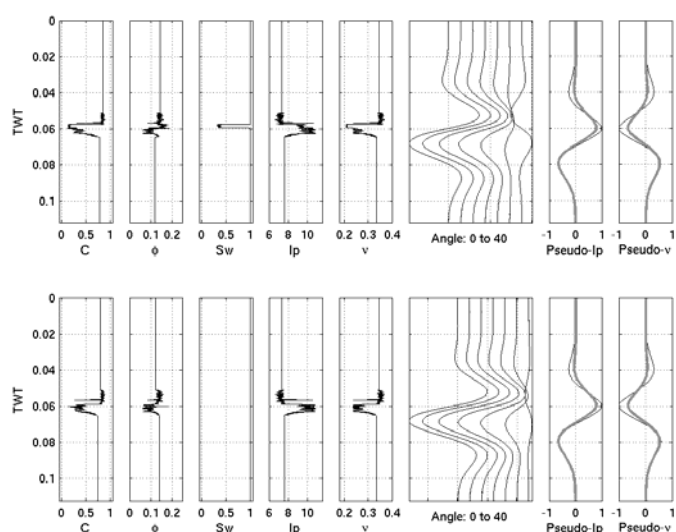


Figure 9. Two pseudo-wells (Well 2, top, and Well 3, bottom) from the gradational model in Figure 4. The exposition is the same as in Figure 7.

Doubling the thickness of the geologic model allows us to resolve the channel better in Wells 2 and 3 (Figure 10). A slight time shift is present in the plots of the attributes from due to slightly different velocity profiles in the corresponding pseudo-well data.

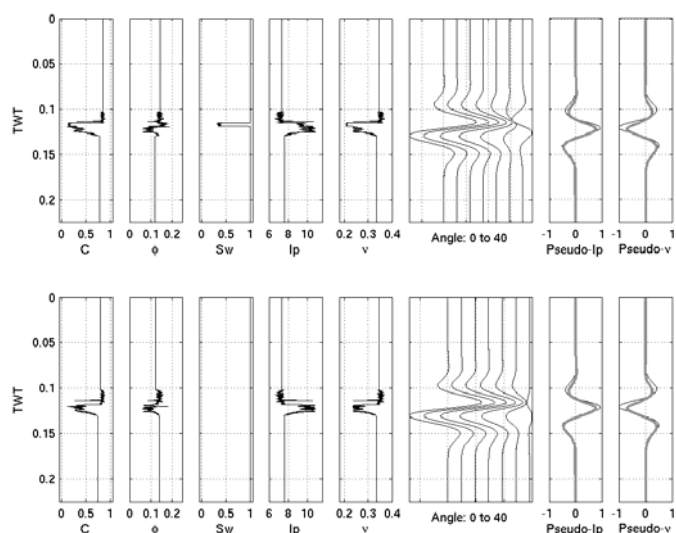


Figure 10. Same as Figure 9, except the thickness of the model is doubled.

Discussion and Conclusions

We demonstrate a method of generating pseudo-wells and synthetic seismic data away from well control based on geologic principles and rock physics. The motivation for using geologic principles is to predict various lithologic sequences systematically in which stratigraphic traps may hold hydrocarbons. This approach is used in traditional basin modeling and, more recently, in high-resolution subsurface geologic modeling software packages, in which templates of depositional sequences are used to construct a volume. Here we show how to use a calibration well to establish a relevant rock physics

model and then consistently populate a geologic model with elastic properties.

Our assumption in synthetic seismic modeling is that if the seismic responses match, then the underlying physical properties match. However, an infinite number of arrangements of physical properties can produce the same seismic response. One solution is to reduce non-uniqueness by revealing the relationship between lithology, fluid, and porosity, as shown above, where an increase in clay content triggers a decrease in porosity and an increase in water saturation. Such relations, if proven valid in a prospect area, may help constrain seismic interpretation. Because we use geologic principles to populate the facies model with clay content values, we limit the number of potential arrangements of the sub-seismic physical properties that control the seismic response.

The focus of our demonstration is to attribute the variation in the rock physics in the geobody to depositional trends. By calculating pseudo wells at equivalent depths, we do not account for depth, mechanical compaction trends, or diagenesis as a function of temperature and pressure. In a more realistic problem with a 3-D geobody with significant depth differences from one location to another, depth and compaction trends certainly should be considered by, e.g., including diagenetic and compaction trends as a function of temperature and pressure.

In this example, we assume that the geologic model includes only clay and quartz. Considering other mineralogic contributions and grain sizes may make modeling more realistic.

Acknowledgments

This work was supported by the Stanford Rock Physics and Borehole Geophysics Project under DOE grant # DE-FG03-99ER14933.

References

- 1) Avseth, P., Mukerji, T., Jorstad, A., Mavko, G., and Veggeland, T., "Seismic reservoir mapping from 3-D AVO in a North Sea turbidite system", *Geophysics*, 2001, **66**, 1157.
- 2) Mukerji, T., Jorstad, A., Avseth, P., Mavko, G., and Granli, J. R., "Mapping lithofacies and pore fluid probabilities in a North Sea reservoir: Seismic inversions and statistical rock physics", *Geophysics*, 2001, **66**, 988.
- 3) Hampson, D. P., Schuelke, J. S., and Quirein, J. A., "Use of multiattribute transforms to predict log properties from seismic data", *Geophysics*, 2001, **66**, 220.
- 4) Walker, R., "Facies Models", Geol. Assn. Can., Toronto, 1984.
- 5) Pratson, L. F., Stroujkova, A., Herrick, D., Boadu, F., and Malin, P., "Predicting seismic velocity and other rock properties from clay content only", *Geophysics*, 2003, **68**, 1847.
- 6) de Groot, P. F. M., Albertus, H. B., Florist, F. J. T., and Campbell, A. E., "Monte Carlo simulation of wells", *Geophysics*, **61**, 631.
- 7) Xu, H., Dai, J., and Dutta, N., "Using rock physics for pseudo well log construction", *73rd Ann. Internat. Mtg., Soc. Expl. Geophys., Exp. Abstr.*, 2003, 1680.

- 8) Gassmann, F., "Über die Elastizität poröser Medien", *Vier. Der Natur Gesellschaft in Zürich*, 1951, **96**, 1.
- 9) Mavko, G., Chan, C., and Mukerji, T., "Fluid substitution: Estimating changes in V_p without knowing V_s ", *Geophysics*, 1995, **60**, 1751.
- 10) Raymer, D. S., Hunt, E. R., and Gardner, J. S., "An improved sonic transit time-to-porosity transform", *Trans. Soc. Prof. Well Log analysts, 21st Annual Logging Symposium*, 1980, Paper P.
- 11) Greenberg, M. L., and Castagna, J. P., "Shear-wave velocity estimation in porous rocks: Theoretical formulation, preliminary verification and applications", *Geophys. Prosp.*, 1992, **40**, 195.
- 12) Castagna, J. P., Batzle, M. L., and Eastwood, R. L., "Relationships between compressional-wave and shear-wave velocities in clastic silicate rocks", *Geophysics*, 1985, **50**, 571.
- 13) Dvorkin, J., and Nur, A., "Elasticity of high-porosity sandstones: Theory for two North Sea datasets", *Geophysics*, 1996, **61**, 1363.
- 14) Van Wagoner, J. C., Mitchum, R. M., Campion, K. M., and Rahmanian, V. D., "Siliciclastic Sequence Stratigraphy in Well logs, Cores, and Outcrops: Concepts for High-Resolution Correlation of Time and Facies", Am. Assoc. Pet. Geol., Tulsa, 1990.
- 15) Brown, A., "Interpretation of Three-dimensional Seismic Data", Am. Assoc. Pet. Geol., Tulsa, 1999.
- 16) Vernik, L., and Nur, A., "Petrophysical classification of siliciclastics for lithology and porosity prediction from seismic velocities", *AAPG Bull.*, 1992, **76**, 1295.
- 17) Nichols, G., "Sedimentology and Stratigraphy", Blackwell Science Ltd, Oxford, 1999.
- 18) Reading, H. G., "Sedimentary Environments: Processes, Facies, and Stratigraphy", Blackwell Science Ltd., Oxford, 1996.
- 19) Marion, D., "Acoustical, mechanical, and transport properties of sediments and granular materials", Ph.D. thesis, Stanford University, 1990.
- 20) Yin, H., "Acoustic velocity and attenuation of rocks: Isotropy, intrinsic anisotropy, and stress induced anisotropy", Ph.D. thesis, Stanford University, 1992.
- 21) Dvorkin, J., and Gutierrez, M. A., "Grain sorting, porosity and elasticity", *Petrophysics*, 2002, **43**, 185.
- 22) Spikes, K. T., and Dvorkin, J. P., "Model-based prediction of porosity and reservoir quality from P- and S-wave data", *Geophys. Res. Lett.*, 2003, **30**, 2029.
- 23) Carman, P.C., "L'écoulement des gaz à travers les milieux poreux", *Bibliothèque des Sciences et des Techniques nucléaires, P.U.F.*, 1961, 52.
- 24) Tixier, M.P., "Evaluation of permeability from electric-log resistivity gradients", *Oil and Gas J.*, 1949.
- 25) Wyllie, M.R.J., and Rose, W.D., "Some theoretical considerations related to the quantitative evaluation of the physical characteristics of reservoir rock from electrical log data", *J. Pet. Tech.*, 1950, **4**, 189.
- 26) Timur, A., "An investigation of permeability, porosity, and residual water saturation relationships for sandstone reservoirs", *The Log Analyst*, 1968, **9**, 8.
- 27) Hilterman, F., "Is AVO the seismic signature of rock properties?", *59th Ann. Internat. Mtg., Soc. Expl. Geophys., Exp Abstr.*, 1989, 559.
- 28) Zoeppritz, K., "Erdbebenwellen VIII B, Ueber Reflexion and Durchgang seismischer Wellen durch Unstetigkeitsflaechen", *Goettinger Nachrichten*, 1919, **I**, 66.